Introduction

White matter hyperintensities in TBI

Random forests for WMH segmentation

Machine learning and pattern recognition techniques have seen increased application for various medical image analysis workflows (see, for example, the annual Workshop on Machine Learning in Medical Imaging held in conjunction with the Medical Image Computing and Computer-Aided Intervention international meeting [1]). Popular techniques such as support vector machines and neural networks have been applied successfully to clinically relevant imaging tasks such as supervised image segmentation (e.g., [2]) and diagnostic prediction (e.g., [3, 4]). Facilitating the current employment of such techniques are the number of available imaging data sets [5] and the public availability of data science packages such as SciPy [6] and the R project for statistical computing [7] and their associated add-on toolkits.

Random forests [8] is a popular machine learning technique that has demonstrated significant utitility for supervised segmentation tasks (e.g., normal human brain segmentation) and other computer vision applications (e.g., human gait detection [9]). In the context of neuropathology, random forest-based paradigms have been employed in the delineation of multiple sclerosis lesions [10], stroke lesions [11], and brain tumors [12–15]. Of note, these latter random forest approaches for brain tumor segmentation have performed well in recent international competitions. In response to the lack of objective comparisons between segmentation algorithms, the Multimodal Brain Tumor Segmentation (BRATS) challenge was initiated in 2012 [16] and has continued every year since under the auspices of the International Conference of Medical Image Computing and Computer Assisted Interventions (MICCAI).

Random forests are conceptually simple [8]. They consist of ensembles of decision trees that are built from training data. Once constructed, data to be classified is "pushed" through each decision tree resulting in a single classification "vote" per tree. These votes are then be used for regression or classification of the data. Although decision trees had been extensively studied previously, the success of employing collections of such weak learners for boosting machine learning performance (e.g., AdaBoost [17, 18]) influenced the similarly sytled conglomeration of decision trees into "forests" with randomized node optimization [19, 20]. Finally, Breiman [8] improved accuracy by random sampling of the training data (i.e., "bagging") resulting in the current random forest framework.

In this work, we develop a concatenated random forest framework with a tailored feature image set for seg-

menting white matter hyperintensities in traumatic brain injury cohorts. Additionally, the entire framework is provided as open source through the well-known open-source ANTs[1] and ANTsR[2] toolkits. Further motivating the investigation of this work is the additional public availability of the TBI cohorts thus permitting full reproducibility of the results reported and discussed.

Materials and Methods

Imaging

Quantitative analysis

Crucial to these supervised segmentation approaches are the creation and selection of "features" as input in conjunction with the ground-truth for model construction. For the targeted application in this work (i.e., white matter hyperintensities), regression/classification are performed at the voxelwise level. In other words, each voxel within the region of interest is sent through the ensemble of decision trees and receives a set of classification votes from each tree permitting a regression or classification solution. Since this procedure is performed at the voxelwise level, intensity information alone is insufficient for good segmentation performance since it lacks spatial context. For example, as pointed out in [21], higher intensities can be found at the periventricular caps in normal subjects which often confounds automated lesion detection algorithms. Other potential confounds include MR signal inhomogeneity and noise. Therefore, even though machine learning and pattern recognition techniques are extremely powerful and have significant potential, just as crucial to outcome is the creative construction and deployment of salient feature images which we detail below.

Feature images for WMH segmentation

Supervised methodologies are uniquely characterized, in part, by the feature images that are used to identify the regions of interest. In Table 1, we provide a list and basic categorization of the feature images used for the initial (i.e., Stage 1—more on the use of multiple random forest stages below) segmentation of the white matter hyperintensities. In addition Figure 1 provides a representation of a set of feature images for a single subject analyzed in this work. Note that in this work we categorize the brain parenchyma with seven labels:

- cerebrospinal fluid (label 1),
- gray matter (label 2),
- white matter (label 3),
- deep gray matter (label 4),
- brain stem (label 5),

Feature type	Image source	Name
Intensities		
normalized/preprocessed	FLAIR, T1, and T2	`Preprocessed`
Symmetric template		
template difference	FLAIR, T1, and T2	`SymmetricTemplateDifference`
contralateral difference	FLAIR, T1, and T2	`ContralateralDifference`
template location indices	FLAIR, T1, and T2	`TemplateIndicesWarped`
Segmentation probabilities		
Pr(cerebrospinal fluid)	T1	`BrainSegmentationPosteriors1`
Pr(gray matter)	T1	`BrainSegmentationPosteriors2`
Pr(white matter)	T1	`BrainSegmentationPosteriors3`
Pr(deep gray matter)	T1	`BrainSegmentationPosteriors4`
Pr(brain stem)	T1	`BrainSegmentationPosteriors5`
Pr(cerebellum)	T1	`BrainSegmentationPosteriors6`
Distance maps		
cerebrospinal fluid	T1 brain segmentation	`NormalizedCsfDistance`
gray matter	T1 brain segmentation	`NormalizedGmDistance`
deep gray matter	T1 brain segmentation	`NormalizedDeepGmDistance`
whole brain	T1 brain segmentation	`NormalizedMaskDistance`
Neighborhood statistics		
mean	FLAIR, T1, and T2	`NeighborhoodMean`
standard deviation	FLAIR, T1, and T2	`NeighborhoodSigma`
skewness	FLAIR, T1, and T2	`NeighborhoodSkewness`

Table 1: List of feature images used for Stage 1 of the proposed white matter hyperintensity segmentation framework. These feature images encompass salient location and intensity information used for voxelwise identification of white matter hyperintensities in TBI. The column on the right provides the names used in the software developed for this methodology and facilitates discussion of the results (cf Figure 2).

- cerebellum (label 6), and

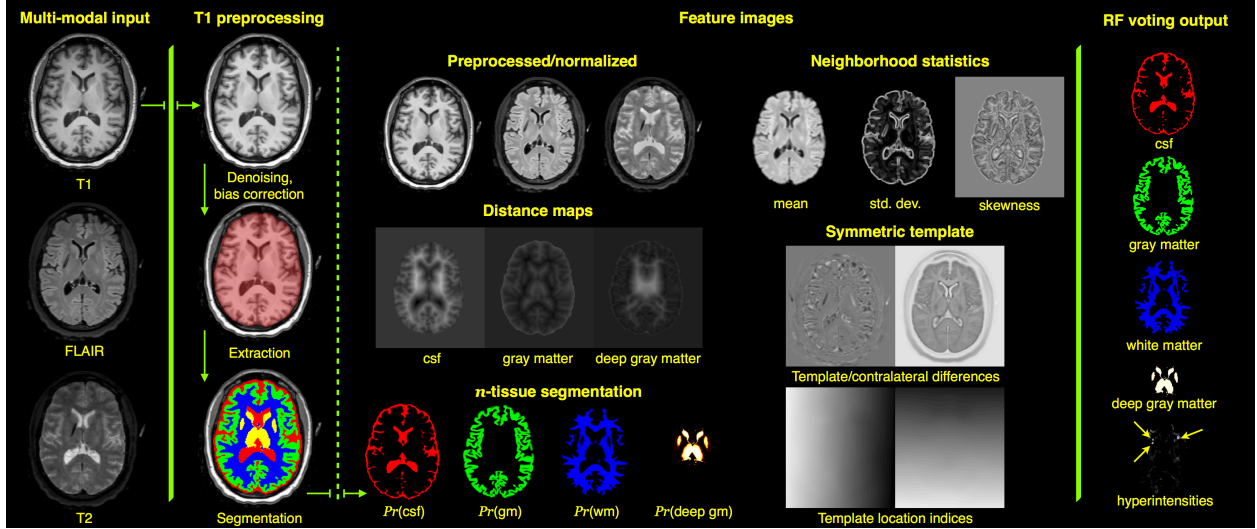- white matter hyperintensities (label 7).

Figure 1: Representation of Stage 1 feature images for subject 01C1019. The FLAIR, T1-, and T2-weighted images are rigidly pre-aligned [22] to the space of the T1 image. The three images are then preprocessed (N4 bias correction [23] and adaptive denoising [24]) followed by application of standard ANTs brain extraction and n-tissue segmentation protocols using the MMRR symmetric template corresponding and priors [25] to the T1 image. The feature images are then generated for voxelwise input to the RF model which results in the voting maps illustrated on the right which gives a probabilistic classification of tissue type. Not shown are the probability and voting images for the brain stem and cerebellum.

As mentioned previously, input for each subject comprises FLAIR, T1-, and T2-weighted acquisitions. The FLAIR and T2 images are rigidly registered to the T1 image using the open-source Advanced Normalization Tools (ANTs) [22]. The aligned images are then preprocessed using the denoising algorithm of [24] followed by N4 bias correction [23] which are then normalized to the intensity range $[0, 1]$. Although we could have used the intensity standardization algorithm of [26], we found that a simple linear rescaling produced better results.

The T1 image is then processed via the ANTs brain extraction and tissue segmentation protocols described in [25] in order to produce a mask for the brain parenchyma and provide probabilistic estimates of the cerebrospinal fluid (csf), gray matter, white matter, deep gray matter, brain stem, and cerebellum. These provide the ground-truth labels for the first six tissue labels given above. The white matter hyperintensities were manually identified by one of the authors (J. R. S.) using the ITK-SNAP tool [27]. Segmentation is performed using the ANTs Atropos tool [28] and multi-model optimal symmetric shape/intensity templates [15] created from

the public MMRR data set [29].

To model the intensity information the first set of images simply includes the preprocessed and normalized intensity FLAIR, T1, and T2 images. We also calculate a set of neighborhood statistics (mean, standard deviation, and skewness) feature images using a radius of one voxel. For each of the normalized images, we calculate the difference in intensities with the corresponding warped template component. Previous success in the international brain tumor segmentation competition [16] was based on an important set of intensity features that were created from multi-modal templates mentioned previously [15]. We employ the same strategy here. For example, the template difference feature image for the FLAIR image, S_{FLAIR} is calculated as:

$$S_{FLAIR} - T_{FLAIR}\left(\phi_b^{-1}\right)$$

where $\phi_b : S \leftrightarrow\underset{b}{\rightsquigarrow} T$ is the transform which maps from the individual subject space to the template space and T_{FLAIR} is the FLAIR template component. Also, to take advantage of the bilateral symmetry of the normal brain (in terms of both shape and intensity), and the fact that the presence of WMH violates that assumption, we use the symmetric templates to compute the contralateral intensity differences as an additional intensity feature. For the FLAIR component, this contralateral difference image is calculated from

$$S_{FLAIR} - S_{FLAIR}\left(\phi_b^{-1}\left(\phi_R\left(\phi_b\right)\right)\right)$$

where ϕ_R denotes a horizontal reflection perpendicular to the mid-sagittal plane of the symmetric template.

The segmentation probability images described above are used as feature images to provide a spatial context for the random forest model prediction step. Additional spatial contextual feature images include the distance maps [30] based on the csf, gray matter, and deep gray matter images. These latter images are intended to help distinguish white matter hyperintensities from false positives induced by the partial voluming at the gray/white matter interface. A third set of images are based on the voxel location within the space of the template. The T1 image of the subject is registered to the T1 template component using a B-spline variant [31] of the well-known ANTs Symmetric Normalization (SyN) algorithm [32]. Since the inverse transform is also derived as part of the registration process, we can warp the voxel index locations back to the space of the individual subject. Note that this is similar in motivation to the work of [33]. However, this previous work lacks the normalization to the standard coordinate system provided by the template to dramatically improve spatial specificity across all subjects.

Stacked (concatenated) random forests for improved segmentation performance

In previous brain tumor segmentation work [15], it was demonstrated that a concatenated supervised approach, whereby the prediction output from the first random forest model serves as partial input for a second random forest model, can significantly improve segmentation performance. We do the same thing for the work described here. The Stage 1 feature images of the training data (as described previously) are used to construct the Stage 1 model. The training data Stage 1 features are then used to produce the voxelwise voting maps via the Stage 1 model. All the Stage 1 features plus the Stage 1 voting maps are used as input to the Stage 2 model. In addition, we use the Stage 1 voting maps as tissue priors for a second application of the Atropos maximum aposteriori algorithm with an additional Markov Random Field spatial prior (MAP-MRF) [28]. However, for the second stage we use all three aligned preprocessed images for a multivariate analysis. The resulting seven posterior probability images constitute a third additional feature image set for Stage 2.

Code and data availability

As pointed out in a recent comprehensive multiple sclerosis lesion segmentation review [34], although the number of algorithms reported in the literature is quite extensive, there were only four publicly available segmentation algorithms at the time of writing of which none are based on supervised learning. As we did for our brain tumor segmentation algorithm [15], all of the code described in this work is publicly available through the open-source ANTs/ANTsR toolkits. Through ANTsR (an add-on toolkit which, in part, bridges ANTs and the R statistical project) we use the `randomForest` package [35] using the default settings with 2000 trees per model and 500 randomly selected samples per label per image.

In addition, similar to our previous offering,[3] we plan on creating a self-encapsulated example to showcase the proposed methodology. The fact that this the data will also be made available through the FITBIR repository along with the ground truth data.

Evaluation protocol overview

In order to evaluate the protocol described, we perform a leave-one-out evaluation using the data acquired from the 24 subjects described above. The Stage 1 feature images were created for all subjects. The initial brain segmentation of each T1 image and the manual white matter hyperintensity tracings were combined to provide the truth labels for the training data. The truth labels are the seven anatomical regions given above.

The leave-one-out procedure is as follows:

- Create Stage 1 feature images for all 24 subjects.

---

[3]https://github.com/ntustison/ANTsAndArboles

- For each of the 24 subjects:
  - sequester the current subject and corresponding feature images.
  - construct the Stage 1 random forest model from the remaining 23 subjects.
  - apply the Stage 1 random forest model to the feature images of the 23 training subjects.
  - the previous step produces the Stage 1 voting maps for all seven labels.
  - for each of the 23 subjects, perform a Bayesian-based segmentation with an MRF spatial prior using the seven voting maps are used as additional tissue priors.
  - construct the Stage 2 random forest model from all the Stage 1 feature images, seven voting maps, and seven posterior probability maps from the previous step.
  - send the sequestered subject through the random forest models for both stages.
  - compare the final results with the manually-defined white matter hyperintensity regions.

Results

Ranking feature importance

After performing the leave-one-out evaluation described at the end of the previous section, we calculated the `MeanDecreaseAccuracy` feature values for each of the 24 subjects $\times$ 2 models per subject $= 48$ total models. This measure (per feature, per model) is calculated during the out-of-bag phase of the random forest model construction and quantifies the decrease in prediction accuracy from omitting the specified feature. In other words, this quantity helps determine the importance of a particular feature and, although we save such efforts for future work, this information provides us with guidance for future feature pruning and/or additions.

The resulting rankings for both Stages are given in Figure 2 where the values for the separate stages are averaged over the entire corresponding model set. In addition, we track the variance for each feature over all models to illustrate the stability of the chosen features during the evaluation. This latter information is illustrated as horizontal errors bars providing the 95th percentile (i.e., $1.96 \times \sigma$). Note that the reader can cross reference Table 1 for identifying corresponding feature types and names.

One can also use these measurements as a type of sanity check. For example, from the Stage 1 plot, one can see that the `MeanDecreaseAccuracy` values for the location indices in the anterior-posterior direction (i.e., `TemplateIndicesWarped1`) are greater than those for either the inferior-superior (i.e., `TemplateIndicesWarped0`) or the left-right (i.e., `TemplateIndicesWarped0`) directions in the space of the symmetric template. This is intuitive since, as discussed previously, manifestation of TBI white matter hyperintensities can often be confused with higher intensities at the periventricular caps in normal subjects [21] whereas there does not seem to be contralateral bias in manifestation of white matter hyperintensities in

Figure 2: Average `MeanDecreaseAccuracy` plots generated from the creation of all 24 random forest models for both Stage 1 and Stage 2 during the leave-one-out evaluation. These plots are useful in providing a quantitative assessment of the predictive importance of each feature. The horizontal error bars provide the 95th percentile (i.e., $1.96 \times \sigma$) and illustrate the stability of the feature importance across the leave-one-out models.

TBI [**???**].

Additionally, it is interesting to note some of the other top performing features for Stage 1. The contralateral difference FLAIR image is highly discriminative over the set of evaluation random forest models. This accords with the known clinical relevance of FLAIR images for identifying white matter hyperintensities and the fact that such pathology does not manifest symmetrically in both hemispheres. Interestingly, the posterior maps for the deep gray matter are extremely important for accurate white matter hyperintensity segmentation. Perhaps the spatial specification of deep gray matter aids in the removal of false positives. Inspection of the bottom of the plots demonstrates the lack of discriminating features associated with the T1 image which is also well-known in the clinical literature.

As described earlier, for Stage 2, we used the output random forest voting maps from Stage 1 as both features themselves and as priors for input to a Bayesian-based segmentation with an additional MRF spatial prior. In Figure 2, the voting maps are labeled as "RFStage1VotingMaps" where the final numeral is associated with the brain parenchymal labeling given previously. Similarly, the additional RF prior segmentation feature probability maps are labeled as "RFBrainSegmentationPosteriors". The Stage 2 feature importance plot follows similar trends as that for Stage 1 with the T1 images not contributing much to the identification of white matter hyperintensity voxels. The initial voting maps from Stage 1 are extremely important with the top 3 being the estimated locations of the 1) gray matter, 2) white matter, and 3) white matter hyperintensities. Since these tissue type can be conflated based on intensity alone it is intuitive that such features would be important.

White matter hyperintensity segmentation evaluation

In Figure 3 are the segmentation comparisons derived from manual segmentations of the same data. Despite the large variability characteristic with manual labelings in related fields [[36];styner2008; @Garcia-Lorenzo:2013aa], such labelings are characteristic of current clinical practices and the methodology proposed herein is readily adapted to refinements in training data. On the left of Figure 3 are the improvement in Dice values over all white matter hyperintensities when comparing the segmentations between the two stages. Performing the second round of supervised learning improves Dice values. One can also note from the right side of Figure 3 that the total lesion load volume illustrates a few subjects that are severe outliers in terms of the number of false positives. The second round helps to correct this issue.
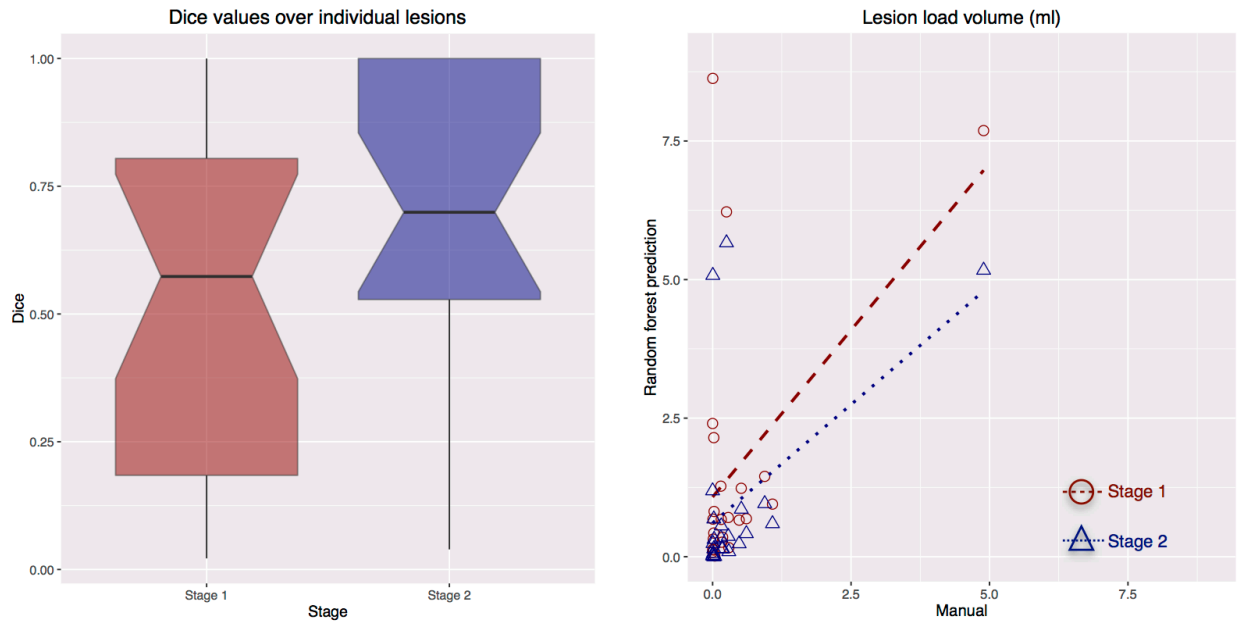
Figure 3: Comparison with manual delineation of white matter hyperintensities. On the left are the calculate Dice values over all white matter hyperintensities. Note the improvement in the Dice metric from the employment of the Stage 2 component of the processing pipeline. (Right) Similar results can be seen by comparing the total lesion load volume between manual and automated detection strategies. Although some outliers are found after the Stage 2 processing in a couple subjects, the number of outliers caused by false positives is significantly with the second stage processing.

References

1. Available at http://mlmi2015.web.unc.edu

2. Bauer, S., Nolte, L.-P., and Reyes, M. "**Fully Automatic Segmentation of Brain Tumor Images Using Support Vector Machine Classification in Combination with Hierarchical Conditional Random Field Regularization**" *Med Image Comput Comput Assist Interv* 14, no. Pt 3 (2011): 354–61.

3. Tong, T., Wolz, R., Gao, Q., Guerrero, R., Hajnal, J. V., Rueckert, D., and Alzheimer's Disease Neuroimaging Initiative. "**Multiple Instance Learning for Classification of Dementia in Brain MRI**" *Med Image Anal* 18, no. 5 (2014): 808–18. doi:10.1016/j.media.2014.04.006

4. Liu, X., Tosun, D., Weiner, M. W., Schuff, N., and Alzheimer's Disease Neuroimaging Initiative. "**Locally Linear Embedding (LLE) for MRI Based Alzheimer's Disease Classification**" *Neuroimage* 83, (2013): 148–57. doi:10.1016/j.neuroimage.2013.06.033

5. Van Horn, J. D. and Toga, A. W. "**Human Neuroimaging as a 'Big Data' Science**" *Brain Imaging Behav* 8, no. 2 (2014): 323–31. doi:10.1007/s11682-013-9255-y

6. Jones, E., Oliphant, T., Peterson, P., and others. "**SciPy: Open Source Scientific Tools for Python**" (2001–2001--): Available at http://www.scipy.org/

7. R Core Team. "**R: A Language and Environment for Statistical Computing**" (2016):

8. Breiman, L. "**Random Forests**" *Machine learning* (2001): 5–32.

9. Viola, P., Jones, M., and Snow, D. "**Detecting Pedestrians Using Patterns of Motion and Appearance**" *International Journal of Computer Vision* 63, (2005): 153–161.

10. Geremia, E., Clatz, O., Menze, B. H., Konukoglu, E., Criminisi, A., and Ayache, N. "**Spatial Decision Forests for MS Lesion Segmentation in Multi-Channel Magnetic Resonance Images**" *Neuroimage* 57, no. 2 (2011): 378–90. doi:10.1016/j.neuroimage.2011.03.080

11. Pustina, D., Coslett, H. B., Turkeltaub, P. E., Tustison, N., Schwartz, M. F., and Avants, B. "**Automated Segmentation of Chronic Stroke Lesions Using LINDA: Lesion Identification with Neighborhood Data Analysis**" *Hum Brain Mapp* (2016): doi:10.1002/hbm.23110

12. Geremia, E., Menze, B. H., and Ayache, N. "**Spatial Decision Forests for Glioma Segmentation in Multi-Channel MR Images**" *Proceedings of MICCAI-BRATS 2012* (2012):

13. Bauer, S., Fejes, T., Slotboom, J., Wiest, R., Nolte, L.-P., and Reyes, M. "**Segmentation of Brain Tumor Images Based on Integrated Hierarchical Classification and Regularization**" *Proceedings of*

MICCAI-BRATS 2012 (2012): 10–13.

14. Zikic, D., Glocker, B., Konukoglu, E., Shotton, J., Criminisi, A., Ye, D. H., Demiralp, C., Thomas, O. M., Das, T., Jena, R., and Price, S. J. "**Context-Sensitive Classification Forests for Segmentation of Brain Tumor Tissues**" *Proceedings of MICCAI-BRATS 2012* (2012): 1–9.

15. Tustison, N. J., Shrinidhi, K. L., Wintermark, M., Durst, C. R., Kandel, B. M., Gee, J. C., Grossman, M. C., and Avants, B. B. "**Optimal Symmetric Multimodal Templates and Concatenated Random Forests for Supervised Brain Tumor Segmentation (Simplified) with ANTsR**" *Neuroinformatics* 13, no. 2 (2015): 209–25. doi:10.1007/s12021-014-9245-2

16. Menze, B. H., Jakab, A., Bauer, S., Kalpathy-Cramer, J., Farahani, K., Kirby, J., Burren, Y., Porz, N., Slotboom, J., Wiest, R., Lanczi, L., Gerstner, E., Weber, M.-A., Arbel, T., Avants, B. B., Ayache, N., Buendia, P., Collins, D. L., Cordier, N., Corso, J. J., Criminisi, A., Das, T., Delingette, H., Demiralp, Ç., Durst, C. R., Dojat, M., Doyle, S., Festa, J., Forbes, F., Geremia, E., Glocker, B., Golland, P., Guo, X., Hamamci, A., Iftekharuddin, K. M., Jena, R., John, N. M., Konukoglu, E., Lashkari, D., Mariz, J. A., Meier, R., Pereira, S., Precup, D., Price, S. J., Raviv, T. R., Reza, S. M. S., Ryan, M., Sarikaya, D., Schwartz, L., Shin, H.-C., Shotton, J., Silva, C. A., Sousa, N., Subbanna, N. K., Szekely, G., Taylor, T. J., Thomas, O. M., Tustison, N. J., Unal, G., Vasseur, F., Wintermark, M., Ye, D. H., Zhao, L., Zhao, B., Zikic, D., Prastawa, M., Reyes, M., and Van Leemput, K. "**The Multimodal Brain Tumor Image Segmentation Benchmark (BRATS)**" *IEEE Trans Med Imaging* 34, no. 10 (2015): 1993–2024. doi:10.1109/TMI.2014.2377694

17. Schapire, R. "**The Strength of Weak Learnability**" *Machine Learning* 5, (1990): 197–227.

18. Freund, Y. and Schapire, R. "**A Decision-Theoretic Generalization of on-Line Learning and an Application to Boosting**" *Journal of Computer and System Sciences* 55, (1997): 119–139.

19. Ho, T. K. "**Random Decision Forests**" *Document analysis and recognition, 1995., proceedings of the third international conference on* 1, (1995): 278–282 vol.1. doi:10.1109/ICDAR.1995.598994

20. Amit, Y. and Geman, D. "**Shape Quantization and Recognition with Randomized Trees**" *Neural Computation* 9, (1997): 1545–1588.

21. Neema, M., Guss, Z. D., Stankiewicz, J. M., Arora, A., Healy, B. C., and Bakshi, R. "**Normal Findings on Brain Fluid-Attenuated Inversion Recovery MR Images at 3T**" *AJNR Am J Neuroradiol* 30, no. 5 (2009): 911–6. doi:10.3174/ajnr.A1514

22. Avants, B. B., Tustison, N. J., Stauffer, M., Song, G., Wu, B., and Gee, J. C. "**The Insight ToolKit Image**

Registration Framework" *Front Neuroinform* 8, (2014): 44. doi:10.3389/fninf.2014.00044

23. Tustison, N. J., Avants, B. B., Cook, P. A., Zheng, Y., Egan, A., Yushkevich, P. A., and Gee, J. C. "**N4ITK: Improved N3 Bias Correction**" *IEEE Trans Med Imaging* 29, no. 6 (2010): 1310–20. doi:10.1109/TMI.2010.2046908

24. Manjón, J. V., Coupé, P., Martí-Bonmatí, L., Collins, D. L., and Robles, M. "**Adaptive Non-Local Means Denoising of MR Images with Spatially Varying Noise Levels**" *J Magn Reson Imaging* 31, no. 1 (2010): 192–203. doi:10.1002/jmri.22003

25. Tustison, N. J., Cook, P. A., Klein, A., Song, G., Das, S. R., Duda, J. T., Kandel, B. M., Strien, N. van, Stone, J. R., Gee, J. C., and Avants, B. B. "**Large-Scale Evaluation of ANTs and FreeSurfer Cortical Thickness Measurements**" *Neuroimage* 99, (2014): 166–79. doi:10.1016/j.neuroimage.2014.05.044

26. Nyúl, L. G., Udupa, J. K., and Zhang, X. "**New Variants of a Method of MRI Scale Standardization**" *IEEE Trans Med Imaging* 19, no. 2 (2000): 143–50. doi:10.1109/42.836373

27. Yushkevich, P. A., Piven, J., Hazlett, H. C., Smith, R. G., Ho, S., Gee, J. C., and Gerig, G. "**User-Guided 3D Active Contour Segmentation of Anatomical Structures: Significantly Improved Efficiency and Reliability**" *Neuroimage* 31, no. 3 (2006): 1116–28. doi:10.1016/j.neuroimage.2006.01.015

28. Avants, B. B., Tustison, N. J., Wu, J., Cook, P. A., and Gee, J. C. "**An Open Source Multivariate Framework for n-Tissue Segmentation with Evaluation on Public Data**" *Neuroinformatics* 9, no. 4 (2011): 381–400. doi:10.1007/s12021-011-9109-y

29. Landman, B. A., Huang, A. J., Gifford, A., Vikram, D. S., Lim, I. A. L., Farrell, J. A. D., Bogovic, J. A., Hua, J., Chen, M., Jarso, S., Smith, S. A., Joel, S., Mori, S., Pekar, J. J., Barker, P. B., Prince, J. L., and Zijl, P. C. M. van. "**Multi-Parametric Neuroimaging Reproducibility: A 3-T Resource Study**" *Neuroimage* 54, no. 4 (2011): 2854–66. doi:10.1016/j.neuroimage.2010.11.047

30. Maurer, C. R., Rensheng, Q., and Raghavan, V. "**A Linear Time Algorithm for Computing Exact Euclidean Distance Transforms of Binary Images in Arbitrary Dimensions**" *Pattern Analysis and Machine Intelligence, IEEE Transactions on* 25, no. 2 (2003): 265–270. doi:10.1109/TPAMI.2003.1177156

31. Tustison, N. J. and Avants, B. B. "**Explicit B-Spline Regularization in Diffeomorphic Image Registration**" *Front Neuroinform* 7, (2013): 39. doi:10.3389/fninf.2013.00039

32. Avants, B. B., Tustison, N. J., Song, G., Cook, P. A., Klein, A., and Gee, J. C. "**A Reproducible Evaluation of ANTs Similarity Metric Performance in Brain Image Registration**" *Neuroimage* 54, no. 3 (2011):

2033–44. doi:10.1016/j.neuroimage.2010.09.025

33. Anbeek, P., Vincken, K. L., Osch, M. J. P. van, Bisschops, R. H. C., and Grond, J. van der. "**Probabilistic Segmentation of White Matter Lesions in MR Imaging**" *Neuroimage* 21, no. 3 (2004): 1037–44. doi:10.1016/j.neuroimage.2003.10.012

34. García-Lorenzo, D., Francis, S., Narayanan, S., Arnold, D. L., and Collins, D. L. "**Review of Automatic Segmentation Methods of Multiple Sclerosis White Matter Lesions on Conventional Magnetic Resonance Imaging**" *Med Image Anal* 17, no. 1 (2013): 1–18. doi:10.1016/j.media.2012.09.004

35. Liaw, A. and Wiener, M. "**Classification and Regression by randomForest**" *R News* 2/3, (2002): 18–22.

36. Grimaud, J., Lai, M., Thorpe, J., Adeleine, P., Wang, L., Barker, G. J., Plummer, D. L., Tofts, P. S., McDonald, W. I., and Miller, D. H. "**Quantification of MRI Lesion Load in Multiple Sclerosis: A Comparison of Three Computer-Assisted Techniques**" *Magn Reson Imaging* 14, no. 5 (1996): 495–505.